Surface and interfacial energies of $Mg_{17}Al_{12}$-Mg system

Fangxi Wang*, Bin Li

Department of Chemical and Materials Engineering, University of Nevada, Reno, NV 89557, USA

* Corresponding author. Email: fangxi.wang@nevada.unr.edu, tel: 775-409-0690

Abstract

For upscale simulation and modeling of magnesium alloys, data of surface and interfacial energies are critical. In this work, we calculated the surface energies of $Mg_{17}Al_{12}$ β-phase with different surface configurations by using molecular dynamic simulations. Surface terminations were carefully selected to calculate the energy of β-phase. The lowest energy surface for each crystallographic plane was determined by varying the surface termination. The results show that surfaces occupied by higher fraction of magnesium atoms generate lower surface energies. The interfacial energy for $Mg_{17}Al_{12}$ β-phase and Mg matrix was calculated as well based on the Burger's orientation relationship. We found that the lowest energy surface of $Mg_{17}Al_{12}$ does not generate the lowest interfacial energy. The interfacial energy for $Mg_{17}Al_{12}$ β-phase and a $\{10\bar{1}2\}$ twin was also calculated. The interfacial energy increases by ~250 mJ/m^2 due to the change in orientation relationship between $Mg_{17}Al_{12}$ and the matrix after twinning.

Key words

$Mg_{17}Al_{12}$ β-phase; Surface termination; Surface energies; Interfacial energy; Atomistic calculations

1. Introduction

Magnesium (Mg) alloys have great potential for applications in automobile, aerospace, and other industries [1] due to their relative low densities and high specific strength [2, 3]. Magnesium-aluminum alloys are the most common commercial Mg alloys and have been widely used as model alloys for research [4]. In these alloys, β-phase ($Mg_{17}Al_{12}$) is the primary equilibrium precipitates in the AZ series Mg alloys. From the literature [5], there are two types of morphology for $Mg_{17}Al_{12}$: continuous precipitation and discontinuous precipitation. The discontinuous precipitation is usually occurred at high grain boundary, and the precipitate growth cellularly to give alternating layers of β-phase and matrix. The continuous precipitation forms large plate β-$Mg_{17}Al_{12}$ at the rest area of the matrix where is no discontinuous precipitation[6], and the β-$Mg_{17}Al_{12}$ prefers the Burgers orientation relationship (OR) with magnesium matrix, i.e., $(0001)_{Mg}||(011)_P, [2\bar{1}\bar{1}0]_{Mg}||[1\bar{1}1]_P$ [5–7].

It is well known that $Mg_{17}Al_{12}$ precipitates influence the mechanical behavior of Mg alloys [cite J.F. Nie's papers]. Robson et al. discussed the effect of precipitates on strengthening considering the precipitate hardening against slip and twinning [8]. They calculated precipitate hardening effect based on Orowan's mechanism. They found that the basal plate precipitates were inefficient to block basal slip, but it hindered twinning growth, because precipitates provided the maximum back-stress and prevented plastic relaxation in the twin. Liao et al. studied the interaction between both prismatic slip and basal slip with a $Mg_{17}Al_{12}$ precipitate in magnesium using molecular dynamics simulations. Their results indicated that both a basal dislocation is able to pass the precipitate without strong interaction, whereas a prismatic dislocation may cut through the precipitate [9, 10]. They also showed that the interface between the precipitate and the matrix was incoherent and the interfacial strength was weak to hinder dislocation slip. Li and Zhang showed that the twinning shear for $\{10\bar{1}2\}\langle 10\bar{1}\bar{1}\rangle$ mode should be zero [11]. Consequently, twin-precipitate interaction should be minimal, which explained why precipitate hardening in magnesium alloy is not as effective as alloys with cubic structures [12]. It was also reported that $Mg_{17}Al_{12}$ phase influences the corrosion behavior [13, 14] because of the free corrosion potential of the β-phase is relative more positive in the electrolyte. Mg/$Mg_{17}Al_{12}$ interfaces can act as a source of crack initiation [15].

Despite the extensive research on precipitation in Mg alloys, key information of surface and interfacial energies are missing. For upscale simulation and modeling, such energies between $Mg_{17}Al_{12}$ and Mg matrix are critically important. Han et al. studied morphological evolution of $Mg_{17}Al_{12}$ phase using phase field simulation. Anisotropy of interfacial

energy and interface mobility, and elastic strain energy was considered [16–18]. How the energy data was calculated was not shown [19]. Hutchinson calculated the interfacial energies in [5],but only the average interfacial energies for $Mg_{17}Al_{12}$/matrix was considered, but the effect of surface termination of $Mg_{17}Al_{12}$ was not considered. Xiao et al.[20] calculated the surface energies of the precipitate for several planes using atomistic simulation but surface termination was not considered as well.

In this paper, we calculated the surface energies of $Mg_{17}Al_{12}$ β-phase with different surface configurations by using atomistic simulation. Surface terminations were carefully selected to calculate the energy of $Mg_{17}Al_{12}$. The interfacial energy between $Mg_{17}Al_{12}$ and Mg matrix was calculated as well based on the Burger's orientation relationship. Because twinning changes the orientation relationship, the interfacial energy between $Mg_{17}Al_{12}$ and matrix after $\{10\bar{1}2\}$ twinning was also calculated.

2. Simulation Method

The EAM [21] interatomic potential for Mg and Al developed by Liu et al. [] was used in our molecular dynamics simulations. This potential has been used in extensive atomistic simulations of physical properties of Mg and Mg alloys [23–26]. Simulation package XMD was used to perform the calculations, and visualization program Ovito [27]was used for graphic presentations.

The Dimensions of the simulation system are 42(X)×42(Y)×11(Z)nm^3 (Fig.1(a)). The orientations are $X-[100], Y-[010], Z-[001]$. The time step size is 3 fs. The system was relaxed for 10,000 time steps (30 ps) to the local minimum potential energy before the surface energy calculation. The temperature for the system was constant at 10 K. Free surfaces were applied to the system. The total number of atoms of the system was about 928,000. To calculate the surface energy of the bottom xy-surface (bottom (001) plane), a box A with the dimension 20(X) × 20(Y) × 3(Z) nm3 (35811 Mg atoms and 25486 Al atoms) was selected in the center of the above relaxed simulation cell, and the average potential energy per atom for each type of atoms was calculated. Another box B with dimension 20(X) × 20(Y) × 5(Z) nm^3 (59019 Mg atoms and 41880 Al atoms) which contains part of the bottom xy-surface was selected, and the average potential energy per atom was calculated. The surface energy γ was given by

$$\gamma = \frac{(E'_{Mg} - E_{Mg}) \times N_{Mg} + (E'_{Al} - E_{Al}) \times N_{Al}}{A}$$

Where E_{Mg} and E_{Al} are the average potential energies per atom for Mg and Al from box A; E'_{Mg} and E'_{Al} are the average potential energies per atom for Mg and Al from box B; N_{Mg} and N_{Al} are the number of Mg and Al atoms in box B; A is the area of the precipitate bottom xy-surface in box B. Fig.1 (b) shows the schematic view of the above calculation methods. The surface energy of each termination was calculated. Then, the system was reoriented to the directions $X-[\bar{2}\bar{1}1], Y-[1\bar{1}1], Z-[011]$, and the surface energies were calculated similarly. The system shows periodicity in all three axes. To find the lowest surface energy termination, we removed the outermost atoms of each surface layer by layer until periodicity is reached, and then calculated the surface energies of different terminations using the above methods. The lowest energy surface termination, as well as the highest energy surface termination can then be determined. Fig.2(a) shows the (010) surface configuration of the precipitate and Fig.2(b) shows the reoriented $(\bar{2}\bar{1}1)$ surface configuration.

In the calculation of the interfacial energy of the bottom xy-surface (bottom (011) plane) of the reoriented precipitate and the Mg matrix, the dimensions of the system are 29(X)×29(Y)×56(Z)nm^3. The system was constructed in the Burger's OR (Fig.3), and six surfaces of the precipitate were the lowest surface energy termination. The system was relaxed for 20,000 time-steps. Free surfaces were applied to the system. The total number of atoms was about 2,244,481. After relaxation, box A and box B with the dimension 10(X) × 10(Y) × 10(Z) nm^3 were selected inside the precipitate and matrix, and the average potential energy per atom for each type of atoms was calculated. Another box C with dimension 20(X) × 20(Y) × 7(Z) which contains the matrix/precipitate interface was selected, and the average potential energy per atom for each type of atoms was calculated as well. The interfacial energy was given by

$$\text{Interfacial enegy} = \frac{(E'_{Mg(m)} - E_{Mg(m)}) \times N_{Mg(im)} + (E'_{Mg(p)} - E_{Mg(p)}) \times N_{Mg(ip)} + (E'_{Al(p)} - E_{Al(p)}) \times N_{Al(ip)}}{A}$$

where $E_{Mg(p)}$ and $E_{Al(p)}$ are the average potential energies per atom for Mg and Al in box A; $E_{Mg(m)}$ is the average potential energy per atom for Mg in box B; $E'_{Mg(p)}$ and $E'_{Al(p)}$ are the average potential energies per atom for Mg and Al in the precipitate in box C; $E'_{Mg(m)}$ is the average potential energy per atom for Mg in the matrix in box C; $N_{Mg(ip)}$ and $N_{Al(ip)}$ are the number of Mg and Al atoms in the precipitate in box C; $N_{Mg(im)}$ is the number of Mg from the matrix in box C; ; A is the area of the matrix/precipitate interface in box C (Fig.4). Then, the matrix was rotated along the $[2\bar{1}\bar{1}0]$ for 90°, and the new interfacial free energies were calculated as well.

3. Results and discussion

The surface termination for the original $Mg_{17}Al_{12}$ β-phase simulation system shows the same periodicity along the three axes. Each repetition contains 12 atomic layers (Fig. 2(a)) (Mg atoms in red and Al atoms in blue). Therefore, we calculated the surface energies for all the 12 layers as bottom surface. We found that the lowest surface energy termination appears when the 8th atomic layer becomes the surface for this structure (Fig. 5(a)), and the surface energy equals 742.7 mJ/m^2. The highest surface energy termination gives the surface energy about 980 mJ/m^2 on the 10th atomic layer (Fig. 5(b)).

For the reoriented β-phase, it shows periodicity along each axis (Fig 2(b)). Along the positive $[1\bar{1}1]$ direction, the structure repeats every 9 atomic layers. However, this case does not show central symmetry as the structure before reorientation. Therefore, the layer structure underneath a specific top or bottom atomic surface will be different, and so will be the surface energies. Fig. 6 shows such differences in detail. Consider the 6th atomic layer becomes the bottom $(1\bar{1}1)$ surface (Fig.6(a)), the underneath layers will be layer 7 to 9 in one period. This termination shows the lowest surface energy of about 775.6mJ/m^2. For the top $(1\bar{1}1)$ surface, the lowest energy termination is the second layer (Fig.6 (c)).

The surface energies result are summarized in Table.1. For the (011) surface, there is only one result because the atom layers show axial symmetry. The (011) surface energy shows a value close to Xiao's result [20] which is 716 mJ/m^2. Other surface energies reported by Xiao [] fall within the range of our calculations. Because no details how surface termination was chosen was provided, discrepancies may incur. Ning et al. calculated the surface energy for (001) plane with atomic layer 1 as the surface by using density functional theory calculation [28]. The value is 799 mJ/m^2, which is slightly higher than the result in our calculation (783 mJ/m^2). For BCC and FCC structures, the closed packed plane surface will usually give the lowest surface energies [29, 30]. $Mg_{17}Al_{12}$ has a BCC structure, the (011) surface indeed provide the lowest surface energy of 715.7 mJ/m^2. In our result, Fig. 6(a) shows the atom layers 6-9 which has a high atomic density gives the lowest surface energies for bottom $(1\bar{1}1)$ plane, but Fig. 6(c) indicates the lowest energy surface termination is not provide by the same layers for top $(1\bar{1}1)$ plane. Therefore, the atom layers with higher atomic density do not necessarily give the lowest surface energies. Additionally, Fig. 5(b) and Fig 6(b,d) show the highest surface energy terminations and these surfaces have more Al atoms. In contrast, surfaces occupied by a higher fraction of magnesium atoms generate lower surface energies.

Lowest surface energies termination is then used to calculate the interfacial energies based on the Burger's OR. After $\{10\bar{1}2\}$ twinning, the OR changes because the Mg matrix was reoriented by ~90 degrees around the zone axis $\langle 2\bar{1}\bar{1}0\rangle$. The interfacial energies between $Mg_{17}Al_{12}$ and a twinned matrix was calculated as well [31]. The results are shown in Table 2. In this case, the lowest energies surface termination generates a relative low interfacial energy about 250 mJ/m^2, which falls in the range of 140~390 mJ/m^2 in [17]. In [5], the interfacial energy was 430 mJ/m^2, and the author showed the effective interfacial energy of nucleation of $Mg_{17}Al_{12}$ was 114 mJ/m^2 by using assessed thermodynamics. Li et al. assumed the interfacial energy of semi-coherent interfaces parallel to the basal planes was 60 mJ/m^2, and 100 mJ/m^2 for incoherent interfaces [19]. Our results show that, for the incoherent interfaces with the Burger's OR, the interfacial energy should be higher than the reported values. Additionally, the lowest energy surface of $Mg_{17}Al_{12}$ does not generate the lowest interfacial energy. The interfacial energy the (011) surface plane of $Mg_{17}Al_{12}$ increases by ~250 mJ/m^2, which indicates that the prismatic plane of the matrix has higher bond strength with the β-phase (011) surface than that of basal plane.

4. Conclusion

In this work, we provided detailed calculations of the surface energies and interfacial energies between $Mg_{17}Al_{12}$ and Mg matrix, using molecular dynamic simulations. Atomic layers were carefully selected to find the lowest surface energy termination for each crystallographic plane of $Mg_{17}Al_{12}$ β-phase. The surface energies vary as the surface structure changes. Generally, surfaces with higher fraction of magnesium atoms generate lower surface energies. The lowest surface energies termination of $Mg_{17}Al_{12}$ does not generate the lowest interfacial energies. The interfacial energy increases by ~250 mJ/m^2 for $Mg_{17}Al_{12}$ β-phase (011) plane after a $\{10\bar{1}2\}$ twinning.

Acknowledgements

Bin Li gratefully thank support from the U.S. National Science Foundation (CMMI-1635088).

5. References

1. Hirsch J, Al-Samman T (2013) Superior light metals by texture engineering: Optimized aluminum and magnesium alloys for automotive applications. Acta Mater 61:818–843. doi: 10.1016/j.actamat.2012.10.044

2. Mordike BL, Ebert T (2001) Magnesium: properties—applications—potential. Mater Sci Eng A 302:37–45.

3. Smola B, Stulíková I, von Buch F, Mordike BL (2002) Structural aspects of high performance Mg alloys design. Mater Sci Eng A 324:113–117. doi: 10.1016/S0921-5093(01)01291-6

4. Frank C (2011) Magnesium Alloys-Design, Processing and Properties. Intech: India

5. Hutchinson CR, Nie J-F, Gorsse S (2005) Modeling the precipitation processes and strengthening mechanisms in a Mg-Al-(Zn) AZ91 alloy. Metall Mater Trans A 36:2093–2105.

6. Celotto S (2000) TEM study of continuous precipitation in Mg–9 wt%Al–1 wt%Zn alloy. Acta Mater 48:1775–1787. doi: 10.1016/S1359-6454(00)00004-5

7. Zhang M-X, Kelly PM (2003) Crystallography of Mg17Al12 precipitates in AZ91D alloy. Scr Mater 48:647–652. doi: 10.1016/S1359-6462(02)00555-9

8. Robson JD, Stanford N, Barnett MR (2013) Effect of Precipitate Shape and Habit on Mechanical Asymmetry in Magnesium Alloys. Metall Mater Trans A 44:2984–2995. doi: 10.1007/s11661-012-1466-0

9. Liao M, Li B, Horstemeyer MF (2013) Interaction between prismatic slip and a Mg17Al12 precipitate in magnesium. Comput Mater Sci 79:534–539. doi: 10.1016/j.commatsci.2013.07.016

10. Liao M, Li B, Horstemeyer MF (2014) Interaction Between Basal Slip and a Mg17Al12 Precipitate in Magnesium. Metall Mater Trans A 45:3661–3669. doi: 10.1007/s11661-014-2284-3

11. Li B, Zhang XY (2016) Twinning with zero twinning shear. Scr Mater 125:73–79. doi: 10.1016/j.scriptamat.2016.07.004

12. Nie J-F (2012) Precipitation and Hardening in Magnesium Alloys. Metall Mater Trans A 43:3891–3939. doi: 10.1007/s11661-012-1217-2

13. Salman SA, Ichino R, Okido M (2010) A Comparative Electrochemical Study of AZ31 and AZ91 Magnesium Alloy. Int J Corros 2010:1–7. doi: 10.1155/2010/412129

14. Zhao M-C, Liu M, Song G, Atrens A (2008) Influence of the β-phase morphology on the corrosion of the Mg alloy AZ91. Corros Sci 50:1939–1953. doi: 10.1016/j.corsci.2008.04.010

15. Lü YZ, Wang QD, Ding WJ, et al (2000) Fracture behavior of AZ91 magnesium alloy. Mater Lett 44:265–268.

16. Han G, Han Z, Alan AL, et al (2013) PHASE FIELD SIMULATION ON MORPHOLOGY OF CONTINUOUS PRECIPITATE Mg $_{17}$ Al $_{12}$ IN Mg-Al ALLOY. Acta Metall Sin 49:277. doi: 10.3724/SP.J.1037.2012.00531

17. Han G, Han Z, Luo AA, Liu B (2014) Three-Dimensional Phase-Field Simulation and Experimental Validation of β-Mg17Al12 Phase Precipitation in Mg-Al-Based Alloys. Metall Mater Trans A 46:948–962. doi: 10.1007/s11661-014-2674-6

18. Han Z, Han G, Luo AA, Liu B (2015) Large-scale three-dimensional phase-field simulation of multi-variant β-Mg17Al12 in Mg–Al-based alloys. Comput Mater Sci 101:248–254. doi: 10.1016/j.commatsci.2015.01.038

19. Li M, Ruijie Z, John A (2010) Modeling Casting and Heat Treatment Effects on Microstructure in Super Vacuum Die Casting (SVDC) AZ91 Magnesium Alloy. In: Magnes. Technol. 2010 Proc. Symp. Held Tms 2010 Annu. Meet. Exhib. Minerals, Metals and Materials Society, pp 623–627

20. Xiao W, Zhang X, Geng WT, Lu G (2013) Atomistic study of plastic deformation in Mg–Al alloys. Mater Sci Eng A 586:245–252. doi: 10.1016/j.msea.2013.07.093

21. Foiles SM, Baskes MI, Daw MS (1986) Embedded-atom-method functions for the fcc metals Cu, Ag, Au, Ni, Pd, Pt, and their alloys. Phys Rev B 33:7983.

22. Liu X-Y, Ohotnicky PP, Adams JB, et al (1997) Anisotropic surface segregation in Al-Mg alloys. Surf Sci 373:357–370.

23. Curtin WA, Olmsted DL, Hector LG (2006) A predictive mechanism for dynamic strain ageing in aluminium-magnesium alloys. Nat Mater Lond 5:875–80. doi: http://dx.doi.org/10.1038/nmat1765

24. Olmsted DL, Jr LGH, Curtin WA, Clifton RJ (2005) Atomistic simulations of dislocation mobility in Al, Ni and Al/Mg alloys. Model Simul Mater Sci Eng 13:371. doi: 10.1088/0965-0393/13/3/007

25. Jones R, Baer D, Danielson M, Vetrano J (2001) Role of Mg in the stress corrosion cracking of an Al-Mg alloy. Metall Mater Trans A 32:1699–1711.

26. Jelinek B, Groh S, Horstemeyer MF, et al (2012) Modified embedded atom method potential for Al, Si, Mg, Cu, and Fe alloys. Phys Rev B 85:245102. doi: 10.1103/PhysRevB.85.245102

27. Stukowski A (2010) Visualization and analysis of atomistic simulation data with OVITO–the Open Visualization Tool. Model Simul Mater Sci Eng 18:015012.

28. Ning H, Zhou Z, Zhang Z, et al (2017) Hydrogen dissociation and incorporation on Mg17Al12(100) surface: A density functional theory study. Appl Surf Sci 396:851–856. doi: 10.1016/j.apsusc.2016.11.041

29. Zhang J-M, Ma F, Xu K-W (2003) Calculation of the surface energy of bcc metals by using the modified embedded-atom method. Surf Interface Anal 35:662–666. doi: 10.1002/sia.1587

30. Zhang J-M, Ma F, Xu K-W (2004) Calculation of the surface energy of FCC metals with modified embedded-atom method. Appl Surf Sci 229:34–42. doi: 10.1016/j.apsusc.2003.09.050

31. Liu B-Y, Wang J, Li B, et al (2014) Twinning-like lattice reorientation without a crystallographic twinning plane. Nat Commun. doi: 10.1038/ncomms4297

Table.1. Surface energies results for $Mg_{17}Al_{12}$ β-phase

	Plane	Direction (layer removing)	Lowest mJ/m^2	Highest mJ/m^2
$Mg_{17}Al_{12}$ without reorient	(001)	[001]	742.7	980.0
$Mg_{17}Al_{12}$ reoriented	$(\bar{2}\bar{1}1)$	$[\bar{2}\bar{1}1]$	789.4	1052.5
	$(\bar{2}\bar{1}1)$	$[2\bar{1}1]$	762.5	952.7
	$(1\bar{1}1)$	$[1\bar{1}1]$	775.6	959.6
	$(1\bar{1}1)$	[111]	761.3	898.2
	(011)	[011]	715.7	1008.6

Table.2. Interfacial energies results for $Mg_{17}Al_{12}$ β-phase/Mg matrix

	Plane (based on β-phase)	Direction (correspond to the surface in Table.1)	Interfacial energy mJ/m^2
$Mg_{17}Al_{12}$/Matrix	(011)	[011]	248~252
$Mg_{17}Al_{12}$/Twin matrix	(011)	[011]	492~496

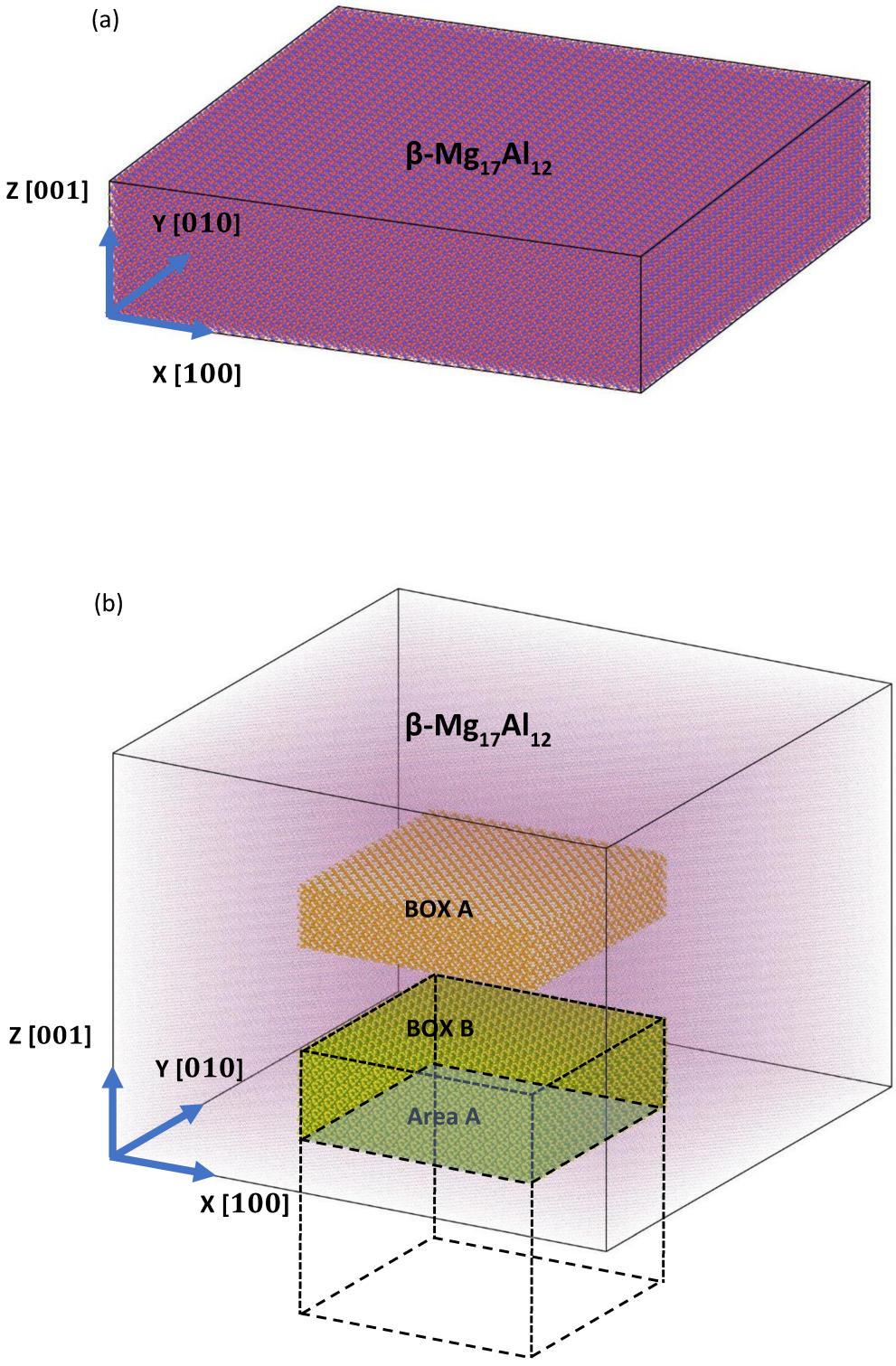

Fig. 1. (a) The 3-D view of the simulation system for $Mg_{17}Al_{12}$. **(b)** The schematic view of the calculation method for surface energies.

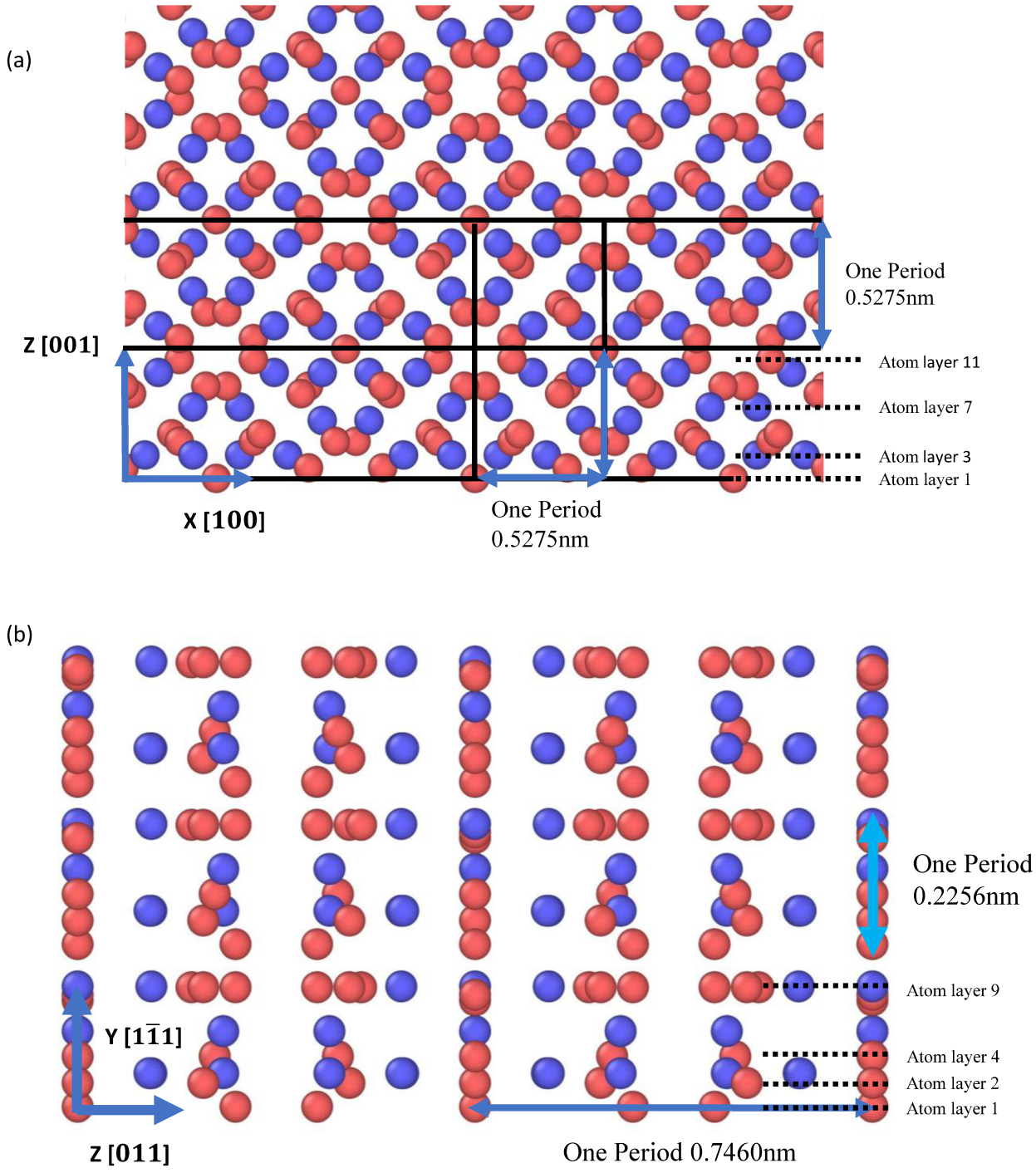

Fig. 2. (a) The (010) surface configuration of the simulation system for $Mg_{17}Al_{12.}$ **(b)** The reoriented ($\bar{2}\bar{1}1$) surface configuration.

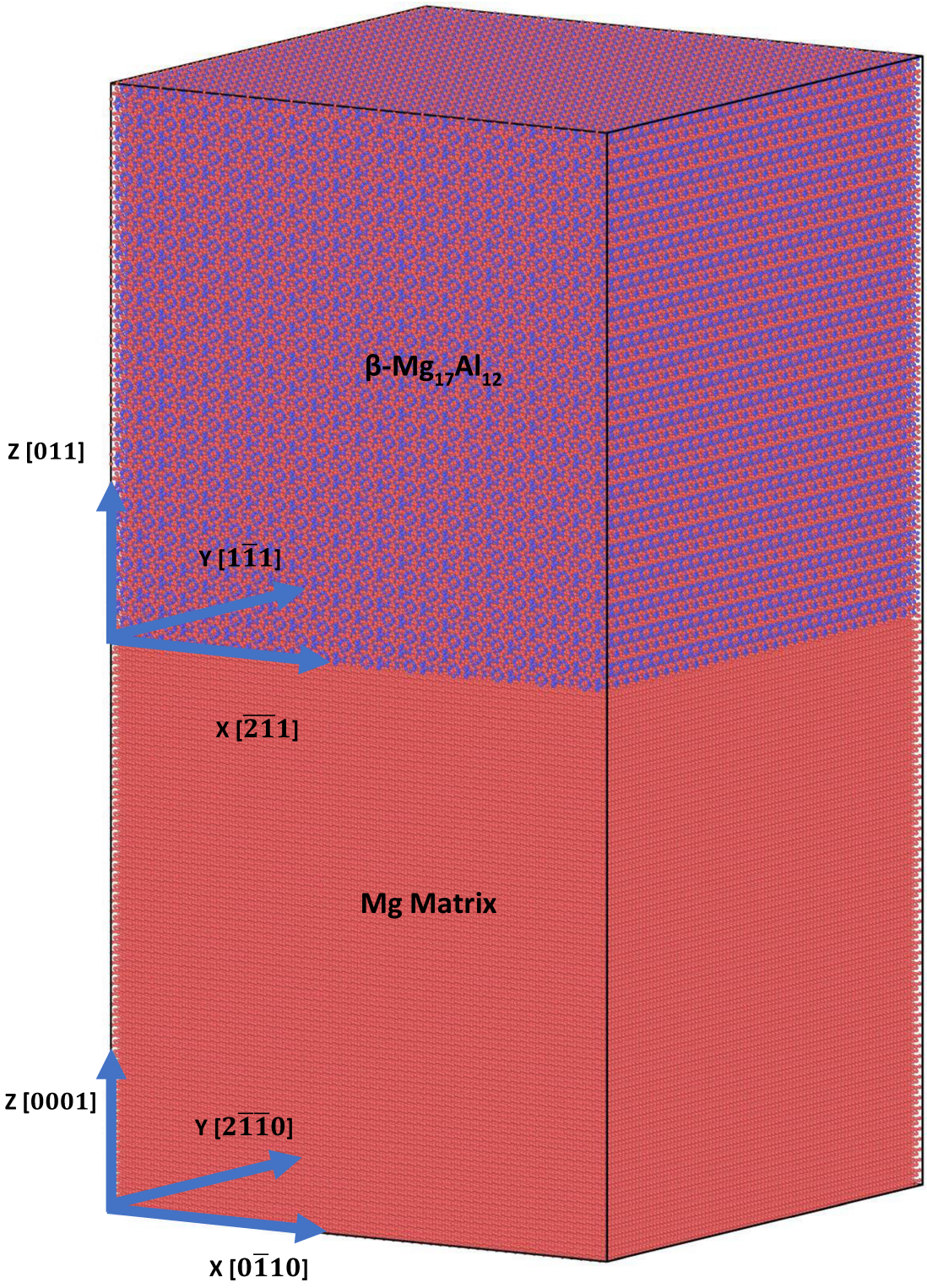

Fig. 3. Schematic 3-D view of the simulation system for interfacial energies calculation with the Burger's OR.

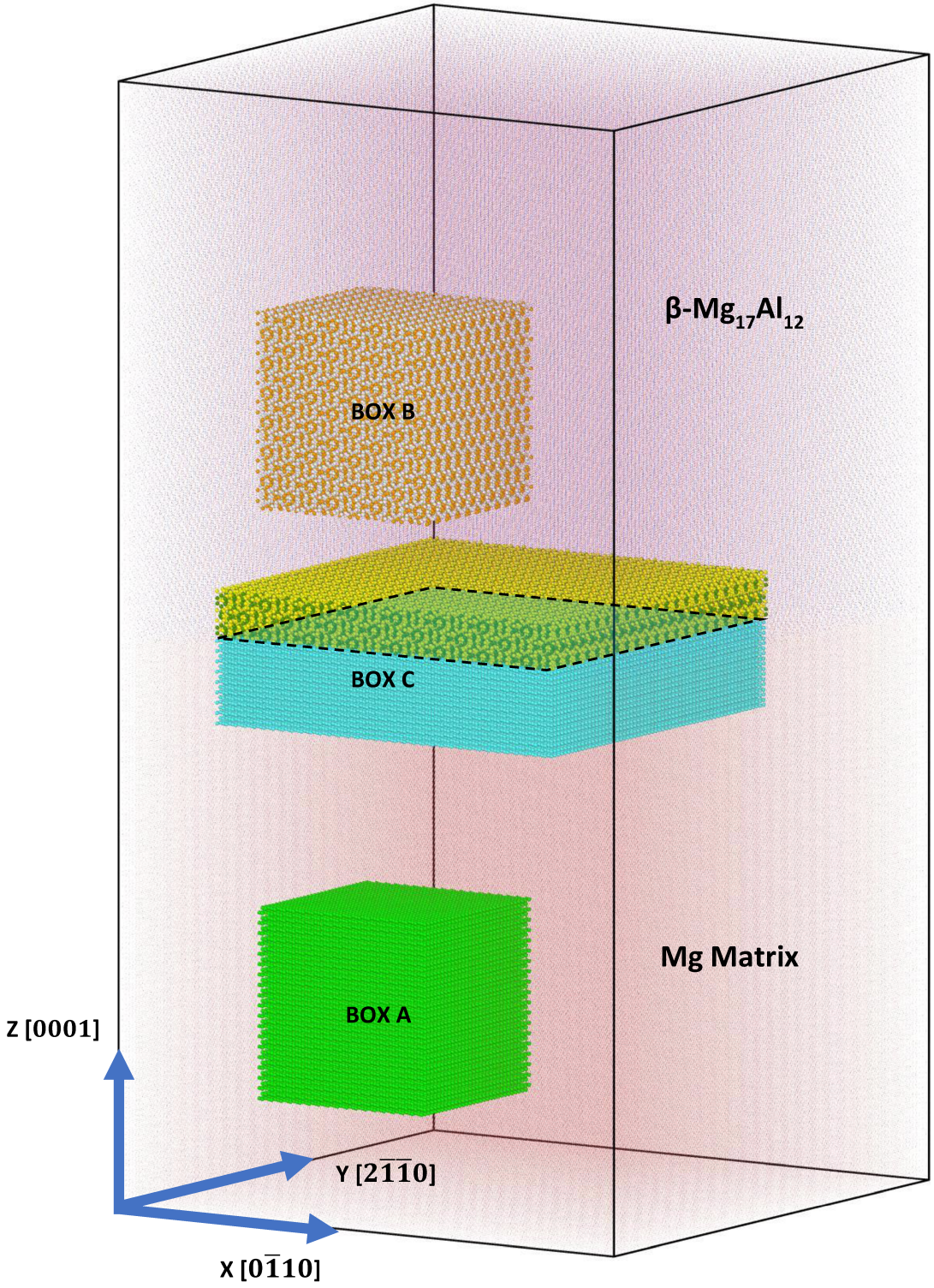

Fig. 4. The schematic view of the calculation methods for interfacial energies calculation.

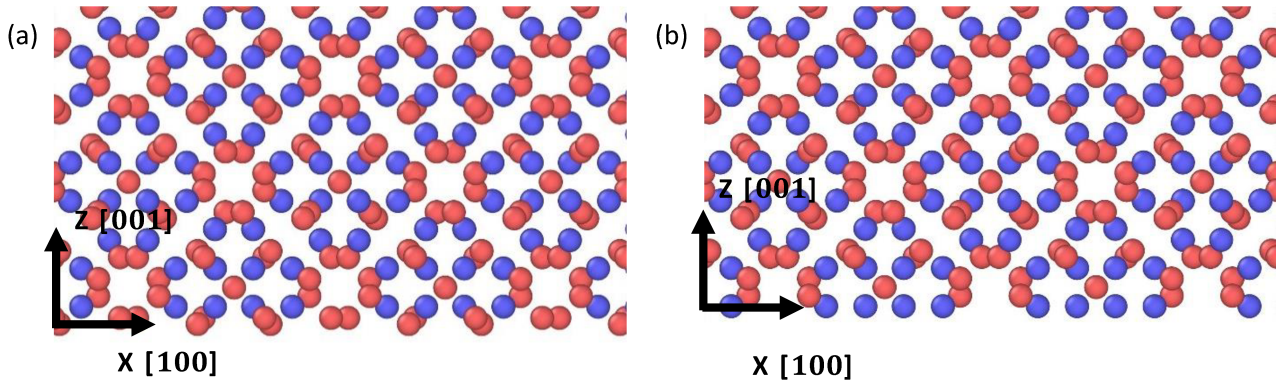

Fig. 5. The side view of the surface termination for $Mg_{17}Al_{12}$ β-phase without reorienting, (001) plane.

(a) Lowest surface energy termination (Atom layer 8; Bottom (001) plane);

(b) Highest surface energy termination (Atom layer 10; Bottom (001) plane).

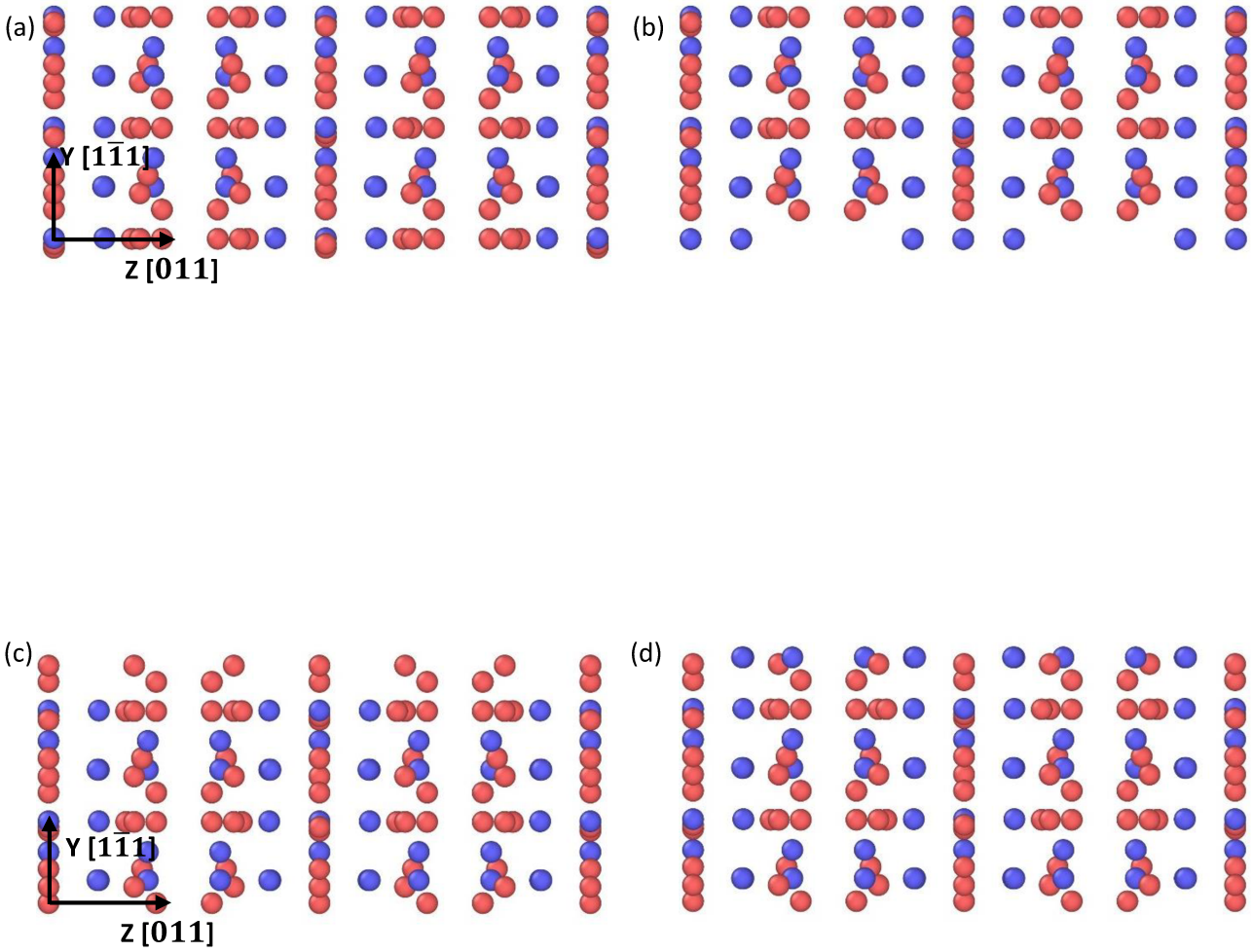

Fig. 6. The side view of the surface termination for reoriented $Mg_{17}Al_{12}$ β-phase, $(1\bar{1}1)$ plane.

(a) Lowest surface energy termination (Atom layer 6; Bottom $(1\bar{1}1)$ plane) for reoriented β-$Mg_{17}Al_{12}$;

(b) Highest surface energy termination (Atom layer 9; Bottom $(1\bar{1}1)$ plane) for reoriented β-$Mg_{17}Al_{12}$;

(c) Lowest surface energy termination (Atom layer 2; Top $(1\bar{1}1)$ plane) for reoriented β-$Mg_{17}Al_{12}$;

(d) Highest surface energy termination (Atom layer 3; Top $(1\bar{1}1)$ plane) for reoriented β-$Mg_{17}Al_{12}$.